The Effect of Alkyl Side-chains on Intercrystallite Ordering in Semiconducting Polymers

Kathryn O'Hara,[1] Christopher J. Takacs, [1, †] Shengjian Liu, [2,⊥] Federico Cruciani, [2] Pierre Beaujuge, [2] Craig J. Hawker, [1] Michael L. Chabinyc[1]

[1]Materials Department, University of California, Santa Barbara, California 93106, United States

[2]Physical Sciences and Engineering Division, KAUST Solar Center, King Abdullah University of Science and Technology, Thuwal 23955-6900, Saudi Arabia

Abstract. The connectivity between ordered domains in semiconducting polymers has been implicated as a bottleneck to charge transport. Crystallites in stiff-chain polymers have been shown to have ordered quasi-epitaxial domain boundaries using electron microscopy, but the factors affecting their formation have not been elucidated. A series of poly (benzo [1, 2-b:4, 5-b′] dithiophene–thieno [3, 4-c] pyrrole-4, 6-dione) (PBDTTPD) polymers with varying sidechains was studied to determine the role of molecular structure on the formation of domain boundaries. Grazing incidence wide angle X-ray scattering revealed the texture of ordered domains in these polymers as function of thickness and thermal processing. High resolution transmission electron microscopy (HRTEM) of thin films revealed that crystallites overlapped in an ordered fashion based on a geometric rule for the length of the crystallographic repeat length and the separation of the backbone by the sidechains. All of the PBDTTPD polymers had polymorphic crystallites due to differences in alkyl stacking that behaved differently depending on their orientation to the substrate during thermal annealing. These results show the importance of domain orientation and boundaries on the morphology of semiconducting polymers.

Introduction

Charge transport within thin films of semiconducting polymers relies on the nanoscale organization of polymers to ensure intermolecular electronic coupling that provides continuous transport pathways. At the molecular level, the two fastest transport directions for polymers are the intramolecular direction along the backbone and the intermolecular direction when their π-conjugated planes overlap.[1,2] In organic electronic devices, such as bulk-heterojunction (BHJ) solar cells[3,4] and thin-film transistors (OTFTs),[5] and thermoelectrics,[6] charge transport occurs over larger length scales than the contour length of the polymer chain (~50 nm with typical molecular weights). Understanding how the longer-range morphology of semiconducting polymers can be affected by their molecular structure is critical to develop structure property relationships.

We study here how the structure of sidechains affects the nanoscale morphology of poly (benzo [1, 2-b:4, 5-b′] dithiophene–thieno [3, 4-c] pyrrole-4, 6-dione) (PBDTTPD) polymers. PBDTTPD is a low band-gap donor-acceptor copolymer which can achieve PCEs of up to 8.5% in BHJs with $PC_{71}BM$.[7–12] The sidechain structure has been shown to have a strong effect on the power conversion efficiency of BHJ solar cells.[8,12–14] Using a combination of X-ray scattering and high-resolution transmission electron microscopy (HRTEM) we reveal how interdomain ordering is impacted by the structure of sidechains in these semicrystalline materials.

There is significant focus on the design of the conjugated backbone of semiconducting polymers to control electronic properties,[15–18] but there is less understanding of how these designs control the solid state ordering over multiple length scales. The connection between processing strategies and the resulting morphologies has been widely studied for semiflexible polymers such as poly(3-hexylthiophene) (P3HT).[19] However, the numerous donor-acceptor copolymers being developed for OPVs and OTFTs typically have much larger, and sterically bulkier, monomer units leading to

stiffer backbones.[20] These stiff backbones have a substantial effect on the phase behavior of the polymer providing a means for thermal processing to aid in tuning morphologies after deposition.[21] Due to the small average grain (domain) size in many semiconducting polymers (~30-50 nm), the connectivity of the ordered and disordered domains will dictate the electrical properties, but there is a general lack of knowledge about the structure of domain boundaries in semiconducting polymers.[22–25]

Close co-facial stacking of the conjugated backbones of polymers is required for efficient hopping between chains, however, solubilizing side-chains are necessary to increase their solubility for processing and can influence the packing structure. The most common sidechains are alkyl groups, both linear and branched,[26] but there are many other chemical variations.[26–30] Conjugated polymers frequently exhibit a packing structure where their semiconducting π-conjugated backbones arrange into closely packed stacks of parallel chains separated by the insulating alkyl side-chains.[21,31] The length and placement of linear alkyl side-chains can lead to closer packing of the main chain through interdigitation,[32] but the structure of branched chains can inhibit close packing.[33] In either case the conjugated backbones have a separation of > 1 nm in the direction of the alkyl stacking preventing strong electronic coupling. The side-chains will also affect the self-assembly and crystallization of polymers. For example, the side-chain density has been correlated with the texture of crystalline domains in films of diketo pyrrolo-pyrrole (DPP)-bithiophene copolymers where a higher density promotes a more face-on orientation of the crystallites.[34]

Gaining detailed information about the structure of grain boundaries in semiconducting polymers is difficult due to their inherent structural disorder. The effect of changes in molecular structure and processing on grain boundaries is therefore often inferred from transport

measurements and modeling.[22,25,35] For example, tie-chains that connect crystalline domains have been cited as the main way to transport charge in P3HT, inferred by the improvement in carrier mobility by increasing the molecular weight[35] and by studies of aligned films.[36,37] Additionally, transport measurements parallel and perpendicular to aligned grain structures have led to the conclusion that electrical properties suffer as the angle of misorientation between adjacent grains increases.[38–40] Direct imaging methods are desirable to fully understand the complexities of molecular arrangement on the nanoscale and the connection with charge transport.

Transmission electron microscopy (TEM) is a powerful tool for determining the orientation of domains in crystalline polymers at the nanoscale. High-resolution TEM (HRTEM) can directly image the crystalline grain boundaries in polymer and small-molecule thin films.[41,42] HRTEM has revealed the domains size in P3HT[43–45] and helped to reveal details about the packing structure of crystalline conjugated polymers.[43,46,47] Maps of the orientation of ordered domains in a thienothiophene polymer, PBTTT, have been measured using dark field transmission electron microscopy (DF-TEM).[48,49] Nanobeam diffraction is emerging as a promising method to image the local order of polymer films.[50,51] These techniques are challenging due to the need to minimize electron-beam induced damage to the sample, but improved direct electron detectors are increasingly available.[52]

Recently, overlapping ordered domains, comparable to quadrites in other synthetic polymers, were discovered in a semiconducting polymer based on dithienosilole-benzothiadizole, Si-PCPDTBT.[46,53] Nonparallel chain packing and homoepitaxy has been observed in other rigid-rod systems such as isotactic polypropylene (iPP),[41,54,55] poly(parapheny1ene benzobisoxazole) (PBZO),[56] and the poly(imide), pyromellitic dianhydrideoxydianiline (PMDA-ODA).[57] HRTEM showed that the backbones of Si-PCPDTBT in ordered domains tend to overlap at a preferred

angle of ≈52°. This quasi-epitaxial relationship was explained a geometric argument given by $\sin(\phi)=d/c$ where c is the crystallographic repeat unit length along the backbone, d is the d-spacing of the alkyl stacking distance, and ϕ is the angle between chains.[53] If the ratio d/c is within possible values, the chains can overlap while maintaining their crystalline order. This cross-hatched morphology in Si-PCPDTBT was also confirmed independently and not found to occur in the carbon-bridged analog, cyclopentadithiophene-benzothiadizole (C-PCPDTBT), or a fluorinated derivative.[46] The benefit of cross-chain structures in insulating polymers, such as iPP, is control of their mechanical properties, but it is unclear if such structures are of significant benefit for charge transport in semiconducting polymers.

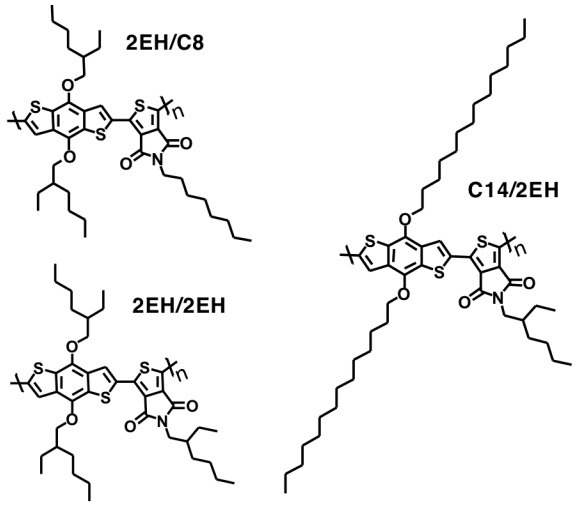

Figure 1. Chemical structures of PBDTTPD polymers with varying sidechain structure where the nomenclature is R_1/R_2 with R_1 on the BDT unit and R_2 on the TPD unit.

We study here the effect of the structure of the backbone on domain boundaries using a series of PBDTTPD polymers (Figure 1). Side-chain induced steric hindrance of the donor and acceptor units in PBDTTPD has been examined in BHJ solar cells, with bulkier side-chains on the donor

unit and a less sterically hindered acceptor unit leading to high power conversion efficiencies.[8,12,14] Variations in the structural order have been observed when the donor and acceptor units were substituted with various branched and linear side-chains, however, the factors driving crystallite orientation are still not well understood.[11] We determined the effect of the alkyl side-chains on intercrystallite order by examining the three different derivatives of PBDTTPD. Our results show that minor variations in side-chain structure drive both texture and the formation of ordered domain overlaps between crystallites. Additionally, the formation of ordered overlapping domains appears to be related to aggregation in solution as films cast from more concentrated solutions lead to a denser cross-hatched morphology observed by HRTEM.

Results and Discussion

Structure of PBDTTPD. The backbone of PBDTTPD allows for varying conformations between heterocycles, but the chain remains linear overall based on models using density functional theory (DFT). Calculations at the B3LYP/6-31G* level of theory were carried out with model oligomers of the main chain with methyl groups at the position of side-chain attachment (Figure 2 and Supplementary Information Figure S1). The conformation of the backbone was examined by setting the dihedral angles between the sulfur atoms on the BDT and TPD units (∠S-C-C-S) such that the sulfur atoms were either *cis* or *trans* as a starting point. The energy-minimized structures show a nearly planar backbone with an undulating, yet linear, structure along the chain axis. The energy minima are close to dihedral angles of 9° and 177° for the *cis* and *trans* conformations. The difference in energy between the lowest energy structure, the all *cis* model, and one with an all *trans* conformation is 11.7 kcal/mol. A model with a mix of *cis* and *trans* conformations that

maintains the linearity of the backbone is 4.8 kcal/mol higher in energy than the all *cis* model. The average difference in energy per bond linking the BDT and the TPD units is ≈1.7 kcal/mol, a relatively small value, suggesting that the backbone could have a mix of angles in the solid state given expected contributions from intermolecular interactions.

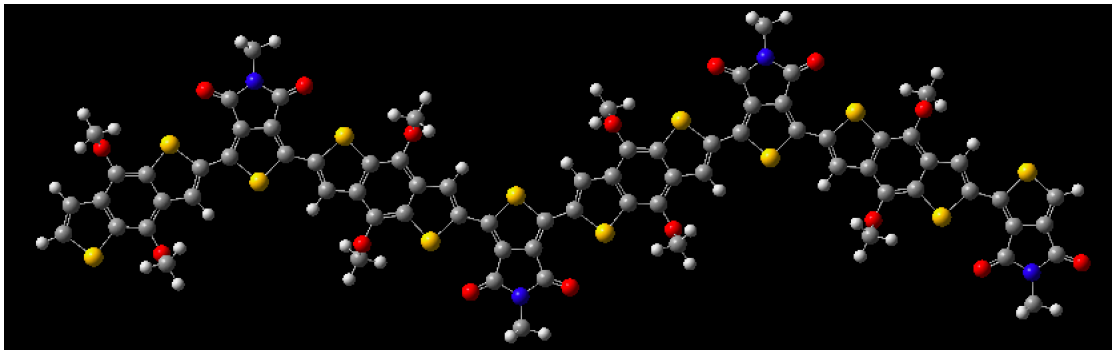

Figure 2. Representative structure from a four repeat unit oligomer showing the undulation in the backbone of the polymer with all sulfur atoms in the trans conformation defined in text. The geometry was optimized at the B3LYP/6-31G* level of theory.

A consequence of the variation in the dihedral angles of the backbone is a difference in the length of the crystallographic repeat length along the backbone direction (Figure S2). If all of the dihedral angles between the sulfur atoms on the BDT and TPD units (∠S-C-C-S) are near 9°, then crystallographic repeat length is 2.44 nm. For alternating dihedral angles of 9 and 177°, the length decreases to 2.40 nm. The shortest repeat unit length of 2.36 nm results when all the dihedral angles are near 177°. Any disorder in the dihedral angle from one value to the other will maintain the linearity of the backbone, but modify the expected crystallographic repeat length by ≈3%. This variation in the length is expected to lead to significant broadening of scattering along the chain

direction in ordered domains (*c*-axis of unit cell) assuming that the backbone is planar in the ordered domains.

Structural Ordering in Thin Films. To investigate the structure of PBDTTPD as a function of sidechain functionalization, thin films were cast under varying conditions for analysis by X-ray scattering and HRTEM. The three polymers PBDTTPD-2EH/C8, 2EH/EH, and C14/2EH had comparable number-average molecular weight by GPC of 17.6, 20.0, and 17.9 kDa respectively (Details in Supporting Information, Figure S2 and Table S1). We note that the 2EH/C8 derivative has a shoulder in the molecular weight distribution, but we do not expect large changes in the local structure because of this difference. The films were cast from solution in chlorobenzene with varying concentration (2, 5, and 10 mg/ml) at a fixed spin-casting conditions (2000 rpm for 45 seconds) to achieve varying thicknesses ranging from ~10 to 60 nm. While the structural ordering was consistent for each polymer, distinct behavior was observed for each as a function of processing conditions.

GIWAXS Shows Differences in Molecular Packing and Texture. Grazing incidence wide-angle X-ray scattering (GIWAXS) shows that the three polymers pack with a lamellar stacking configuration, but with differences in the alkyl stacking distance depending on the side-chains (Figure 3). The alkyl stacking peaks of the polymers can be observed by GIWAXS in the low-*q* region from 0.2 to 0.3 $Å^{-1}$ and a feature assigned to π-π stacking is in the range of *q*=1.7 to 1.8 $Å^{-1}$. Face-on crystallites are characterized by the appearance of an in-plane alkyl stacking peak and out-of-plane π-π stacking peak, whereas the edge-on (and near to edge-on) crystallites produce out-of-plane alkyl and in-plane π-π stacking peaks (Figure 3 and Figure S3). The scattering patterns and *d*-spacings are in good agreement with previously reported values for the polymers (Table 1),[8,34] and we discuss the detailed differences between the polymers below.

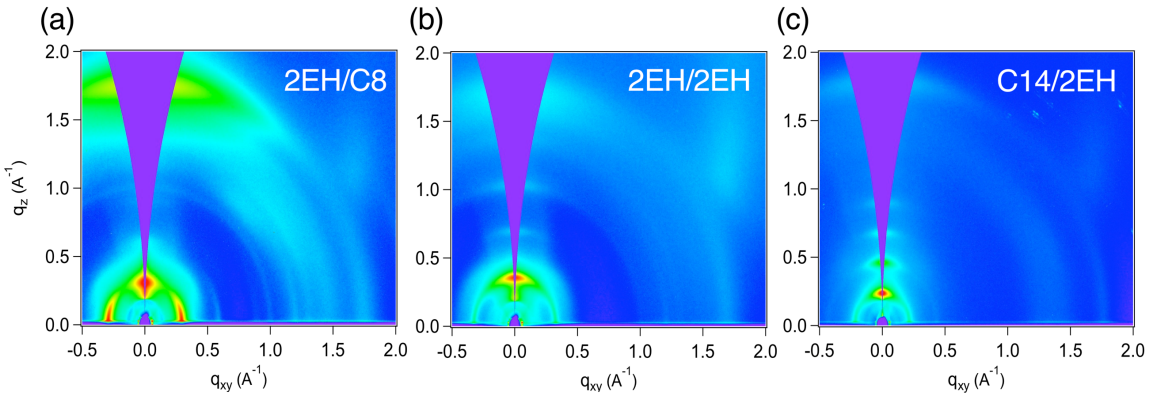

Figure 3. Images of GIWAXS of as-cast 30 nm-thick films of PBDTTPD with varying sidechains: **(a)** 2EH/C8, **(b)** 2EH/2EH, **(c)** C14/2EH. The polymers were dissolved at a concentration of 5 mg/mL in chlorobenzene

Small differences in alkyl stacking distances are observed for the edge-on and face-on crystallite populations within each film (Table 1). Changes in structure and texture have been observed upon thermal annealing some systems,[58–61] but the structure of in-plane and out-of-plane crystallites in thin films are frequently observed, or assumed, to be the same. In the near edge-on crystallite population of PBDTTPD, the alkyl stacking distances of the three derivatives are 4-11% smaller than the face-on population suggesting that there is a small structural difference between the two populations in each polymer. Additionally, the number of observable *a*-axis peaks vary between the in-plane and out-of-plane populations indicating differences in the quality of ordering (Figure 3). All three derivatives show four orders of diffraction in the out-of-plane direction. The in-plane 2EH/C8 shows peaks assignable to 5 orders of diffraction consistent with the (100) planes, C14/2EH shows two orders and 2EH/2EH has only a first order alkyl stacking peak in-plane. The in-plane crystallite coherence length L_c, based on a Scherrer analysis ($L_c=2\pi K/\Delta q$, where K is a dimensionless shape factor and Δq is the diffraction peak FWHM), for the 3 derivatives is near 30

nm. The out-of-plane L_c varies between 15 and 30 nm providing a bound on the domain size (Table 1). There is a nearly negligible difference of at most ≈1% in the π-π stacking distances between the edge-on and face-on populations.

Table 1. Parameters extracted from X-ray scattering from as-cast 30 nm-thick films of the PBDTTPD polymers from 5 mg/mL solutions in chlorobenzene. The fraction of near edge-on crystallites is taken from χ of ≈0 to 30°, the near face-on crystallites are taken between 60-90° with the remaining fraction of crystallites off-axis.

	edge-on crystallites				***face-on crystallites***			
polymer	alkyl stacking (Å)	coherence length (Å)	π-stacking (Å)	fraction (%)	alkyl stacking (Å)	coherence length (Å)	π-stacking (Å)	fraction (%)
2EH/C8	20.5	150	3.57	19	21.2 Å	330	3.61 Å	66
2EH/2EH	17.8	310	3.68	49	19.1 Å	270	3.73 Å	28
C14/2EH	26.7	260	3.53	62	28.8 Å	280	3.55 Å	24

Differences in the texture of the crystalline domains are observed based on the nature of the side-chains. The approximate crystallite texture was computed using the alkyl stacking peak; we note that at grazing incidence, the true specular scattering cannot be collected and thus the texture is underestimated by a fraction of the population of edge-on crystallites.[62] The population of near edge-on crystalline is defined by the intensity from χ of 0° to 30° whereas the near face-on crystallites are taken between 60-90° (Table 1 & Figure S4). The 2EH/C8 derivative is predominately face-on with 66% face-on and 19% edge-on crystallites. The 2EH/2EH and C14/EH derivatives have a similar distribution with the former containing 27% face-on and 49% edge-on crystallites, and the latter with 24% face-on and 62% edge-on crystallites. In a previous study using films cast from chlorobenzene and a 1-chloronapthalene additive, the attachment of branched side-chains to the BDT unit promoted a face-on texture, while linear sidechains resulted in a more edge-

on texture.[8] Our results are consistent with this work as the most face-on derivative, 2EH/C8, has a branched side-chain on the donor unit and linear on the acceptor unit, while the most edge-on material is C14/2EH, which has a linear chain on the donor and branched on the acceptor.

HRTEM Reveals Ordered Overlap of Crystalline Domains. Phase-contrast HRTEM images of PBDTTPD using the periodicity of packing of the alkyl side-chains in face-on orientation provide a real-space picture of how crystallites arrange and connect in thin films. Details of the imaging conditions and processing methods along with the raw images are given in the Supporting Information (Figures S5-S11). The domain boundaries of polymers are defined by a combination of processing methods and molecular structure.[53,62,63] We, and others, have previously observed ordered overlaps of crystalline domains in films of Si-PCPDTBT using HRTEM that depend on geometric rule based on molecular structure.[46,63] By using a series of polymers with the same backbone and varying sidechain substitution, we expected that if ordered overlaps of domains occur in PBDTTPD, then variations in the crossing angle, ϕ, should be observed due to the difference in alkyl stacking distance. In order to satisfy the prediction that $\sin(\phi)=d/c$, the alkyl stacking distance (d) must be smaller than the length of the crystallographic repeat unit of the main polymer chain (c) (Figure 4). Therefore, extended side-chains that increase the alkyl stacking distance will prevent overlap for a given backbone. While this simple geometric model of chain overlap is a starting point for understanding how cross-chain structures may fit together, it is an oversimplification because it first assumes a planar conjugated backbone and it also assumes that there is enough volume to accommodate the sidechains with close-overlaps. For PBDTTPD we speculate that the crossing occurs at the BDT unit based on steric considerations as has been suggested previously based on favorable oxygen-sulfur interactions between chains.[64] The range

of sidechain structures examined here allow us to test this simple prediction to determine if it is indeed a good guideline for materials design relative to carrying out detailed simulations.[46]

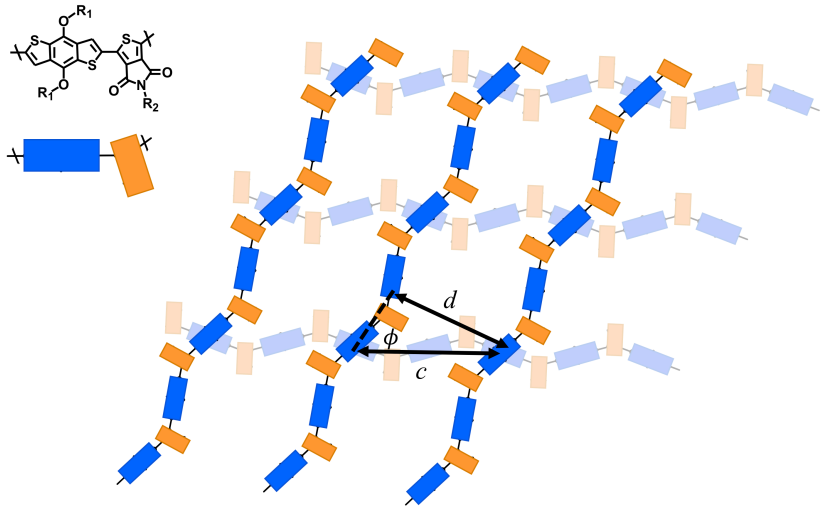

Figure 4. Schematic of overlapping chains of PBDTTPD where the faded chains represents a crystallite below the crystallite with bold chains. A simple model for overlapping domains gives $\sin(\phi)=d/c$ where the alkyl stacking distance (d) and the length of the crystallographic repeat unit of the main polymer chain (c). The sidechains, R_1 and R_2, are omitted for clarity, but their steric interactions play an important role in whether such structures are possible for a given polymer.

Ordered overlapping crystalline domains are observed readily for PBDTTPD-2EH/C8 derivative in as-cast thin films (~15 nm). Cross-hatched features due to overlapping crystallites are observed in HRTEM images (500x500 nm) during examination of data sets covering areas over 50 μm^2 (Figure 5). Because HRTEM images in transmission through the film, there can be domains that are in molecular contact or separated through the thickness. When the overlap of the face-on crystallites constitute a grain boundary it can be classified as a lateral chain rotation in the classification proposed in previous studies.[56] There are overlaps of face-on PBDTTPD crystallites at an angle near 56° along with overlaps other angles near the edges of crystallites. We find that the 56° angle is in reasonable agreement with our geometric model that predicts an overlap angle of ≈59° using a repeat length of 2.4 nm (Figure 5). A schematic showing a model of chains overlapping at the BDT unit is given as Figure 4; we propose this structure based on the ability of the alkoxy sidechains to face away from each other on π-stacked chains preventing steric interactions. It has also been suggested in literature that the π-stacking in PBDTTPD could be stabilized by overlap of the donor units at an angle of ≈60° due to sulfur-oxygen interactions.[64] Overlapping crystallites in Si-PCPDTBT were predicted to cross at the benzodiathiazole unit based on comparable steric argument[53] that was confirmed by molecular modeling.[46]

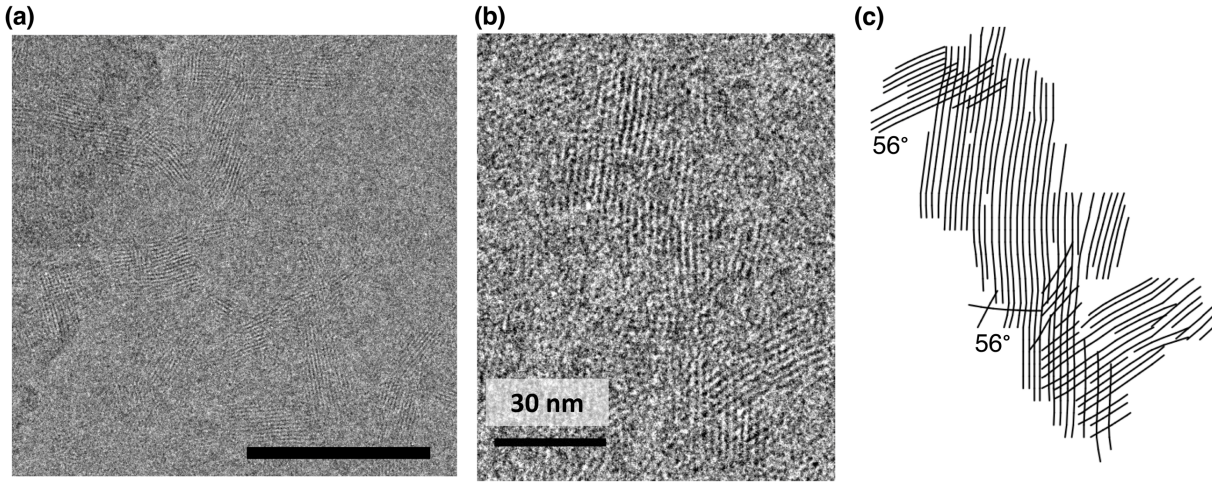

Figure 5. (a) HRTEM image of PBDTTPD-2EH/C8 thin film (15 nm) cast from 2 mg/mL solution. Scale bar is 100 nm **(b)** HRTEM at higher magnification showing overlapping crystallites **(c).** Line drawing representation of chains in the ordered crossings extracted from HRTEM image.

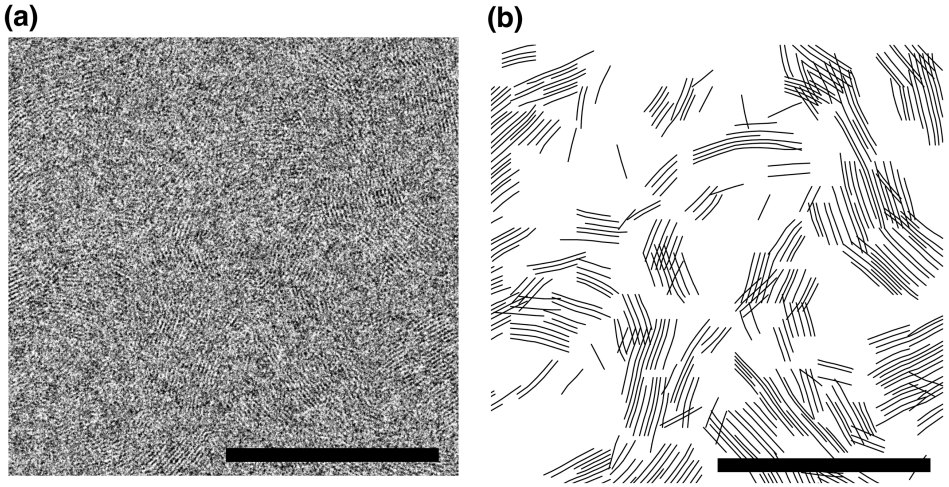

Figure 6. (a) HRTEM image of PBDTTPD-2EH/2EH thin film cast from 5 mg/mL solution **(b)** Line drawing representation of chains in the ordered crossings extracted from HRTEM image. Scale bars are 100 nm.

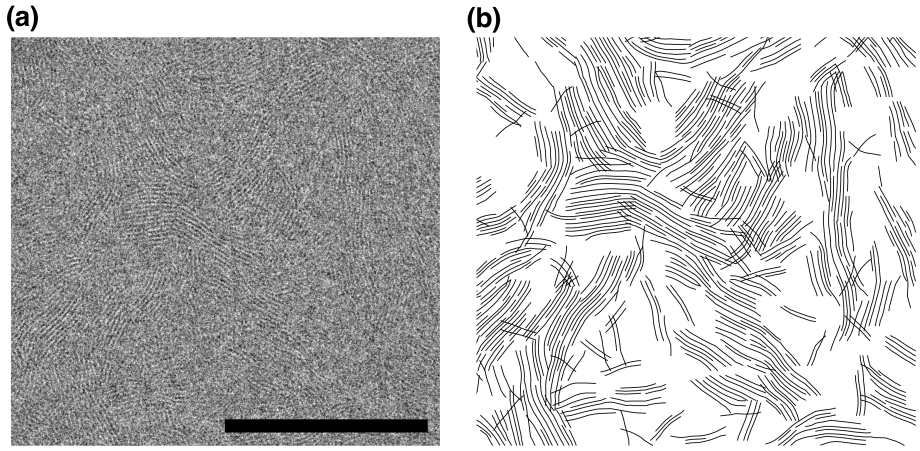

Figure 7. **(a)** HRTEM image of PBDTTPD-C14/2EH thin film (~15 nm) cast from 2 mg/mL solution **(b)** Line drawing representation of chains in the ordered crossings extracted from HRTEM image. Scale bars are 100 nm.

HRTEM images reveal that the clear overlapping domains observed for PBDTTPD-2EH/C8 are not present in the 2EH/2EH and C14/2EH derivatives. The fraction of face-on oriented crystallites determined by GIWAXS is close to 25% for these materials. The crystallites are only observed in about 25% of the area of the images for 2EH/2EH (Figure 6, Figure S8). The simple geometric model predicts a crossing angle of 48° and some regions of overlapping crystallites occur near this angle (~52°). Overlap of the crystallites, however, occurs at the edges of crystallites over smaller distances (~10 nm) for 2EH/2EH instead of overlap over the entire crystallite width (~30 nm) as observed for 2EH/C8. Despite the prediction of the geometric model for overlap, the bulkiness of the branched ethyl-hexyl side-chain on the TPD acceptor unit may frustrate the packing at domain boundaries. The geometrical model does not predict a crossing for the C14/2EH derivative because the alkyl stacking distance (2.9 nm) is larger than the crystallographic repeat unit (2.4 nm); HRTEM images do not show overlapping domains, but features similar to those observed for the

naphthalene diimide-thiophene co-polymer, P(T2NDI-OD) (Figure 7).[58,63] The texture of the crystallites from GIWAXS was 24% face-on suggesting that the face-on crystallites be segregated to the top, or bottom, of the film. An estimate of the thickness of the face-on crystallites is provided by the width of the out-of-plane π-π stacking peak centered at $q_z \approx 1.78$ Å. The coherence length of the face-on population is ≈6.3 nm; in a film thickness of around 15 nm, it is therefore plausible that a thin layer of edge-on crystallites forms above or below the face-on crystallites. Such a stratification has also been found in films of P(T2NDI-OD) further suggesting the similarities between the morphology of the two materials.[65]

The presence of branched versus linear side-chains will affect the ability of the π-faces of the polymers to pack closely in a non-parallel arrangement of the main chains. In the case of Si-PCPDTBT, the acceptor unit does not have side-chains, which minimizes steric congestion at the proposed point of overlap, and the Si-C bonds at the bridgehead of the CPD unit allowed for close packing of the π-faces.[46,53,66] The situation becomes more complex for polymers with side-chains on both the donor and acceptor units. Here, PBDTTPD-2EH/C8 and PBDTTPD-2EH/2EH are both predicted to overlap, however, only PBDTTPD-2EH/C8 exhibits a significant fraction of domain overlaps. This observation suggests that a sterically unhindered acceptor unit is an important determinant of whether efficient crystallite overlap will occur. In addition, while the model predicts the single most probable overlap angle, local fluctuations in *d*-spacing and other structural features, such as the conformation of the chain and dislocations, will lead to a distribution of angles. As an example, a distribution in the angle of grain boundaries has been observed in pyromellitic dianhydride-oxydianiline (PMDA-ODA) and attributed to fluctuations in the crystallographic angle, γ, of the unit cell.[57] While we cannot expect that our reductive model

could capture these features, it does appear to be a reasonable approximation based on our HRTEM data.

Dependence of morphology on casting concentration. The type of domain boundaries formed in a film should strongly depend on their thickness. First, simple geometric factors may prohibit overlapping domains depending on the size of the crystallites relative to the thickness of the film. Second, if the increase in thickness is achieved by changing the concentration of polymer in solution, then aggregation of the chains in solution during the casting process should also have a major impact on the morphology.[67] The cross-hatched morphology in Si-PCPDTBT was found to develop after spin-coating, but was not present after high-temperature (HT) rubbing, which was hypothesized to occur because Si-PCPDTBT aggregated more strongly in solution.[46] It is likely that the formation of cross-chain structures and the resulting crystallite texture in thin films of PBDTTPD is related to aggregation in solution. We therefore expected to see differences in the resulting morphology because the 2EH/2EH and C14/2EH derivatives of PBDTTPD were soluble in chlorobenzene at room temperature, whereas solutions of the 2EH/C8 derivative were heated to achieve dissolution and cooled to room temperature before casting.

The overlap density of face-on crystallites increases in PBDTTPD-2EH/C8 as the film thickness increases and is likely connected to aggregation in solution. By varying the solution concentration between 1 and 10 mg/ml and keeping the spin-casting conditions identical, the film thickness could be varied from ≈10 to 60 nm. The percentage of face-on and edge-on crystallites determined by GIWAXS changes in the films of PBDTTPD-2EH/C8 as the solution used for spin-casting becomes more concentrated (Table S2). When the solution is the most concentrated (10 mg/ml), the crystallites in the film have a distribution of 73% face-on and 14% edge-on, while in the most dilute solution (1 mg/ml) have a distribution of 26% face-on and 64% edge-on. For thin

films (~15 nm) from a 2 mg/ml solution of 2EH/C8 in chlorobenzene, individual crystallites are observed to overlap and intersect (Figure 8a and Figure S5). By doubling the thickness to 30 nm with a 5 mg/ml solution, we find regions in HRTEM where more than two crystallites overlap with the same angle of ≈60° further suggesting that chains are epitaxially arranging on one another (Figure 8b, Figure S6). Doubling the thickness again to 60 nm with a 10 mg/ml solution results in a very and densely crosshatched morphology (Figure S7); the power spectrum shows that the crystallites have an overall isotropic orientation, but overlap at angles around 60° can still be observed locally. These data suggest that aggregation in solution may promote formation of the overlapping domain boundaries.

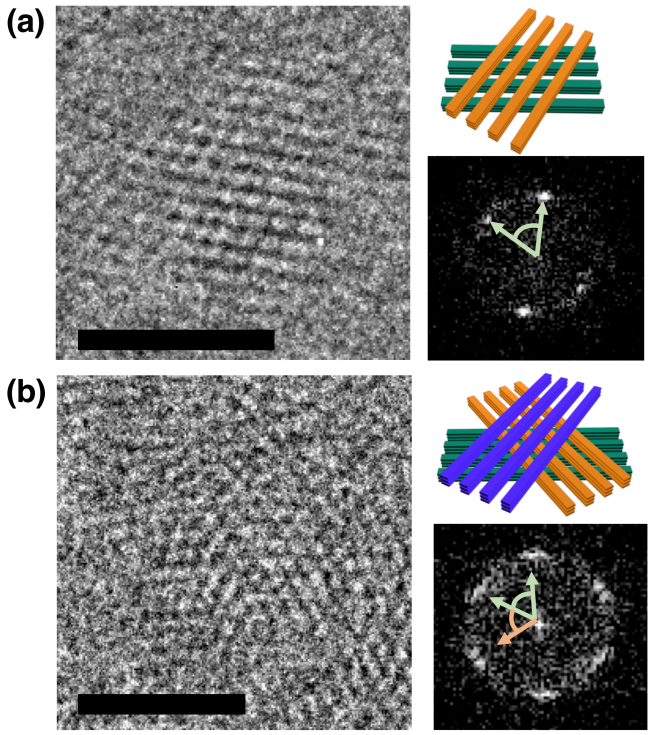

Figure 8. HRTEM images and Fourier transform showing overlapping crystallites of PBDTTPD:2EH/C8 **(a)** 2 crystallites in 15 nm thick film and **(b)** 3 crystallites 30 nm thick film where each is oriented at a relative angle of ≈60°. The scale bar is 20 nm.

Increasing the film thickness through the use of more concentrated solutions does not result in an increase in crystallite overlap for the 2EH/2EH and C14/2EH derivatives (Figure S9 and S11). However, 2EH/2EH and C14/2EH also have a lower percentage of face-on character compared to 2EH/C8 at comparable casting concentration. Detailed examination of the change in texture of the ordered domains with solution concentration for 2EH/2EH revealed only minor changes compared to 2EH/C8 (Table S2). Spin casting a thin film from the most concentrated solution (10 mg/mL) leads to a 45% edge-on and 27% face-on character with a similar distribution in the film cast from 1mg/mL solution. This further suggests the influence of concentration for the behavior of the 2EH/C8 derivative.

Thermal annealing reveals structural polymorphs. We expected that the differences in overlaps of ordered domains could impact the way the films respond to thermal annealing. The crossed crystallites may act as physical crosslinks and change the way the film expands and contracts during heating and cooling due to the necessity of two domains changing together. While sufficient material was not available for quantitative mechanical testing to determine if the observed cross-change structures behaved as physical cross-links, the process of floating the thin films onto TEM grids provided some qualitative insight into the mechanical behavior. Floating of the thinnest films (10-15 nm) was more successful for PBDTTPD-2EH/C8, which has significant crystallite overlap, versus films of the 2EH/2EH and C14/2EH derivatives, which were prone to shatter during transfer to the TEM grid. We note that this behavior is an empirical observation and cannot rule out other defects as the origin of the difference in mechanical behavior. Because we expected that crystallites with differing texture would respond differently to thermal annealing, we examined the evolution of the structure of the three PBDTTPD derivatives using GIWAXS.

GIWAXS *in-situ* thermal annealing revealed how the packing structure of the crystallites depended on the texture of the film. Here, the polymer films were heated to 250°C for 30 min followed by slow cooling at 5-10°C/min to room temperature. This temperature was chosen because it was below the decomposition temperature and still high enough that morphological rearrangements could occur in a relatively short time scale (See Supporting Information, Figure S12). The population of near edge-on and face-on crystallites did not dramatically change for any of the PBDTTPD derivatives, but the alkyl stacking distances in the two populations did show significant differences. This contrasts the behavior of systems like P(T2NDI-OD) where polymorphism occurs with a change in texture.[59,68]

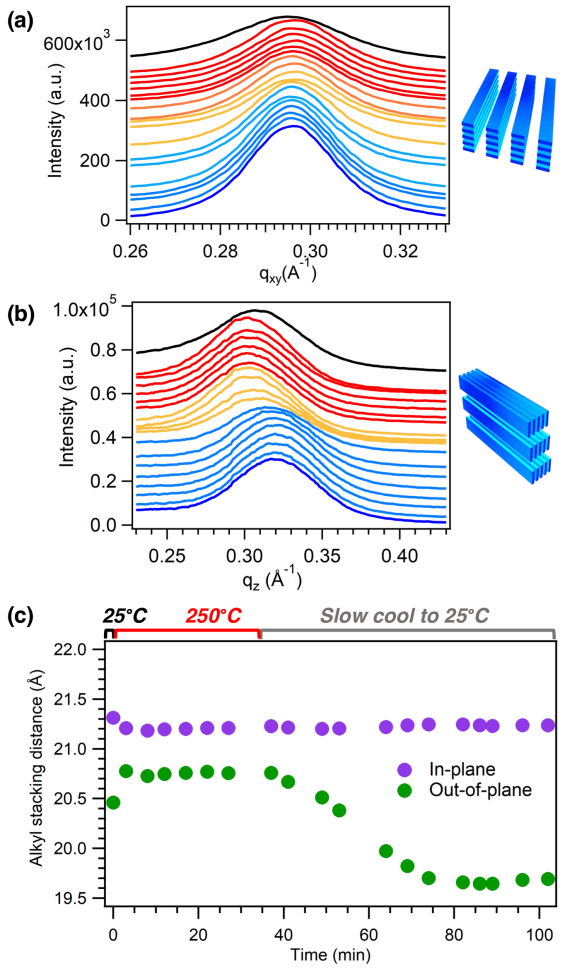

Figure 9. Results of GIWAXS *in-situ* heating of PBDTTPD-2EH/C8 at 250°C for 30 min followed by slow cooling to room temperature. 1D line-cuts of the alkyl stacking peak (a) in-plane and (b) out-of-plane, and (c) evolution of alkyl stacking distance during heating and cooling for the in- and out-of-plane direction.

For the PBDTTPD-2EH/C8, the face-on and edge-on crystallites show a different response to thermal annealing as evidenced by the change in *d*-spacing during heating and cooling (Figure 9). Minimal change is observed in the in-plane direction; the alkyl stacking distance is 2.13 nm before annealing and 2.12 nm after slow cooling. The out-of-plane alkyl stacking distance shows an initial expansion from 2.05 to 2.08 nm during heating followed by a contraction to 1.97 nm which is a 4% reduction. Thermal expansion, or contraction, has been observed during the initial annealing of many semiconducting[21] and non-conjugated stiff chain polymers[69] depending on the density of the sidechains and their structure. Here, the contraction suggests that the density of the sidechains increases upon thermal annealing, which is likely caused by small conformational rearrangements of the branched sidechains.

PBDTTPD-C14/2EH and PBDTTPD-2EH/2EH have a distribution of polymorphic crystallites that behave differently upon thermal annealing. The in-plane alkyl stacking of PBDTTPD-C14/2EH exhibits simple 4% contraction during annealing from 2.89 to 2.78 nm. This small contraction that occurs upon reaching 250° C and only shifts slightly upon cooling is likely due to minor rearrangements of the linear tetradecyl side-chains on the BDT donor unit. The crystallites that are oriented near the edge-on direction behave differently than the face-on population. The out-of-plane alkyl stacking peak at q = 0.234 Å^{-1} (d =2.68 nm) splits into 2 resolved peaks at q = 0.228 Å^{-1} (d = 2.82 nm) and q = 0.248 Å^{-1} (d = 2.53 nm) at 250° C (Figure S13). The width of the initial peak suggests that both populations were present in the as-cast film and then evolve upon heating and cooling. Upon cooling, both peaks show a contraction in *d*-spacing from 2.82 to 2.55 nm (q = 0.247 Å^{-1}) for the lower-q peak and 2.53 to 2.35 nm (q = 0.266 Å^{-1}) for the higher q peak and eventually merge into a single broad feature at room temperature. Similar behavior is also observed for PBDTTPD-2EH/2EH (Figure S14). While the face-on crystallites show little change

in *d*-spacing (1.92 nm) during heating and cooling, the edge-on crystallite show a contraction in the spacing. While heating at 250°C, the out-of-plane alkyl stacking peak splits into 2 peaks at q=0.336 Å^{-1} (d=1.86 nm) and q=0.360 Å^{-1} (d= 1.74 nm) and evolve into one population with a scattering feature at q=0.369 Å^{-1} (d =1.70 nm) at room temperature (Figure S14).

The behavior of the three polymers suggests the role of domain boundaries and physical stress on the ordered populations. For PBDTTPD-C14/2EH and PBDTTPD-2EH/2EH, the more edge-on orientated crystallites contract upon heating and cooling by ~7% and ~9 % respectively whereas there are smaller shifts of the face-on population. PBDTTPD-2EH/C8 has similar behavior with a smaller contraction for the edge-on crystallites. This difference suggests that the in-plane population is constrained by the interaction of the film with the substrate as well as the interdomain connectivity; the edge-on population has one free interface whereas the in-plane population does not. HRTEM does not show the same degree of overlap of the crystallites for the three polymers suggesting that ordered domain boundaries are not the sole origin of the difference in the populations. It is likely that the physical constraints of the substrate may prevent contraction in the in-plane crystallites in the polymers.

Conclusion

We have shown that the morphology of thin films of a series of PBDTTPD polymers is affected by several factors including the molecular structure, processing, and aggregation in solution. Our results test the utility of a previously proposed model[46,53] based on molecular geometry to provides a guide of possible structures for ordered domain boundaries. HRTEM of thin films of PBDTTPD-2EH/C8 showed ordered overlap of domains around the predicted angle of ~60° along with other

angles of overlap. Crystallites of PBDTTPD-2EH/2EH were also predicted to have ordered overlapping domains, but the results from HRTEM were not pronounced and attributed to the presence of branched instead of linear chain on the acceptor unit. Our results here do confirm the role of the sidechains in dictating these ordered domain boundaries. The dependence of the formation of these boundaries in films PBDTTPD-2EH/C8 on the concentration of the casting solution suggests a further route to control the hierarchical nanostructure in polymer thin films.

A surprising observation in our study was the presence of polymorphic crystallites in all three PBDTTPD derivatives that behaved differently during thermal annealing depending on their orientation to the substrate. Thermal annealing and *in-situ* GIWAXS showed that the edge-on crystallites had larger changes in their structure (> 4% change) than face-on crystallites without large changes in the texture. These results contrast other systems where polymorphs have been observed after large changes in texture of the ordered domains.[58,59] These observations suggest that mechanical properties, i.e. stresses in the films, may have a role in determining the packing structure after thermal annealing.

Supporting Information. Polymer characterization, additional GIWAXS and transmission electron microscopy images, UV-Vis spectroscopy of annealed films, and analysis of GIWAXS.

Corresponding Author

Michael L. Chabinyc mchabinyc@engineering.ucsb.edu

Present Address

⊥Shengjian Liu, School of Chemistry and Environment, South China Normal University, Guangzhou 510006, P. R. China

† Stanford Synchrotron Radiation Lightsource, Menlo Park, CA, USA 94025

Acknowledgments

This work was also supported through the NSF DMREF program (DMR 1436263). Polymer synthesis was funded by Baseline Research Funding from King Abdullah University of Science and Technology (KAUST). The MRL Shared Experimental Facilities are supported by the MRSEC Program of the NSF under Award No. DMR 1720256. Use of the Stanford Synchrotron Radiation Lightsource, SLAC National Accelerator Laboratory, is supported by the U.S. Department of Energy, Office of Science, Office of Basic Energy Sciences, under Contract DE-AC02-76SF00515.

REFERENCES

(1) Olivier, Y.; Niedzialek, D.; Lemaur, V.; Pisula, W.; Müllen, K.; Koldemir, U.; Reynolds, J. R.; Lazzaroni, R.; Cornil, J.; Beljonne, D. 25th Anniversary Article: High-Mobility Hole and Electron Transport Conjugated Polymers: How Structure Defines Function. *Adv. Mater.* **2014**, *26* (14), 2119–2136. https://doi.org/10.1002/adma.201305809.

(2) Coropceanu, V.; Cornil, J.; da Silva Filho, D. A.; Olivier, Y.; Silbey, R.; Brédas, J.-L. Charge Transport in Organic Semiconductors. *Chem. Rev.* **2007**, *107* (4), 926–952. https://doi.org/10.1021/cr050140x.

(3) Dou, L.; You, J.; Hong, Z.; Xu, Z.; Li, G.; Street, R. A.; Yang, Y. 25th Anniversary Article: A Decade of Organic/Polymeric Photovoltaic Research. *Adv. Mater.* **2013**, *25* (46), 6642–6671. https://doi.org/10.1002/adma.201302563.

(4) Hou, J.; Inganäs, O.; Friend, R. H.; Gao, F. Organic Solar Cells Based on Non-Fullerene Acceptors. *Nat. Mater.* **2018**, *17* (2), 119–128. https://doi.org/10.1038/nmat5063.

(5) Sirringhaus, H. 25th Anniversary Article: Organic Field-Effect Transistors: The Path Beyond Amorphous Silicon. *Adv. Mater.* **2014**, *26* (9), 1319–1335. https://doi.org/10.1002/adma.201304346.

(6) Russ, B.; Glaudell, A.; Urban, J. J.; Chabinyc, M. L.; Segalman, R. A. Organic Thermoelectric Materials for Energy Harvesting and Temperature Control. *Nat. Rev. Mater.* **2016**, *1* (10), 1–14. https://doi.org/10.1038/natrevmats.2016.50.

(7) Zou, Y.; Najari, A.; Berrouard, P.; Beaupré, S.; Réda Aïch, B.; Tao, Y.; Leclerc, M. A Thieno[3,4- *c*]Pyrrole-4,6-Dione-Based Copolymer for Efficient Solar Cells. *J. Am. Chem. Soc.* **2010**, *132* (15), 5330–5331. https://doi.org/10.1021/ja101888b.

(8) Cabanetos, C.; El Labban, A.; Bartelt, J. A.; Douglas, J. D.; Mateker, W. R.; Fréchet, J. M. J.; McGehee, M. D.; Beaujuge, P. M. Linear Side Chains in Benzo[1,2- *b* :4,5- *b* ′]Dithiophene–Thieno[3,4- *c*]Pyrrole-4,6-Dione Polymers Direct Self-Assembly and Solar Cell Performance. *J. Am. Chem. Soc.* **2013**, *135* (12), 4656–4659. https://doi.org/10.1021/ja400365b.

(9) Piliego, C.; Holcombe, T. W.; Douglas, J. D.; Woo, C. H.; Beaujuge, P. M.; Fréchet, J. M. J. Synthetic Control of Structural Order in *N* -Alkylthieno[3,4- *c*]Pyrrole-4,6-Dione-Based Polymers for Efficient Solar Cells. *J. Am. Chem. Soc.* **2010**, *132* (22), 7595–7597. https://doi.org/10.1021/ja103275u.

(10) Bartelt, J. A.; Douglas, J. D.; Mateker, W. R.; Labban, A. E.; Tassone, C. J.; Toney, M. F.; Fréchet, J. M. J.; Beaujuge, P. M.; McGehee, M. D. Controlling Solution-Phase Polymer Aggregation with Molecular Weight and Solvent Additives to Optimize Polymer-Fullerene Bulk Heterojunction Solar Cells. *Adv. Energy Mater.* **2014**, *4* (9), 1301733. https://doi.org/10.1002/aenm.201301733.

(11) El Labban, A.; Warnan, J.; Cabanetos, C.; Ratel, O.; Tassone, C.; Toney, M. F.; Beaujuge, P. M. Dependence of Crystallite Formation and Preferential Backbone Orientations on the Side Chain Pattern in PBDTTPD Polymers. *ACS Appl. Mater. Interfaces* **2014**, *6* (22), 19477–19481. https://doi.org/10.1021/am505280a.

(12) Constantinou, I.; Lai, T.-H.; Klump, E. D.; Goswami, S.; Schanze, K. S.; So, F. Effect of Polymer Side Chains on Charge Generation and Disorder in PBDTTPD Solar Cells. *ACS Appl. Mater. Interfaces* **2015**, *7* (48), 26999–27005. https://doi.org/10.1021/acsami.5b09497.

(13) Dyer-Smith, C.; Howard, I. A.; Cabanetos, C.; El Labban, A.; Beaujuge, P. M.; Laquai, F. Interplay Between Side Chain Pattern, Polymer Aggregation, and Charge Carrier Dynamics in PBDTTPD:PCBM Bulk-Heterojunction Solar Cells. *Adv. Energy Mater.* **2015**, *5* (9), 1401778. https://doi.org/10.1002/aenm.201401778.
(14) Savikhin, V.; Babics, M.; Neophytou, M.; Liu, S.; Oosterhout, S. D.; Yan, H.; Gu, X.; Beaujuge, P. M.; Toney, M. F. Impact of Polymer Side Chain Modification on OPV Morphology and Performance. *Chem. Mater.* **2018**, *30* (21), 7872–7884. https://doi.org/10.1021/acs.chemmater.8b03455.
(15) Dou, L.; Liu, Y.; Hong, Z.; Li, G.; Yang, Y. Low-Bandgap Near-IR Conjugated Polymers/Molecules for Organic Electronics. *Chem. Rev.* **2015**, *115* (23), 12633–12665. https://doi.org/10.1021/acs.chemrev.5b00165.
(16) Yao, H.; Ye, L.; Zhang, H.; Li, S.; Zhang, S.; Hou, J. Molecular Design of Benzodithiophene-Based Organic Photovoltaic Materials. *Chem. Rev.* **2016**, *116* (12), 7397–7457. https://doi.org/10.1021/acs.chemrev.6b00176.
(17) Nielsen, C. B.; Turbiez, M.; McCulloch, I. Recent Advances in the Development of Semiconducting DPP-Containing Polymers for Transistor Applications. *Adv. Mater.* **2013**, *25* (13), 1859–1880. https://doi.org/10.1002/adma.201201795.
(18) Son, H. J.; Carsten, B.; Jung, I. H.; Yu, L. Overcoming Efficiency Challenges in Organic Solar Cells: Rational Development of Conjugated Polymers. *Energy Environ. Sci.* **2012**, *5* (8), 8158. https://doi.org/10.1039/c2ee21608f.
(19) Tremel, K.; Ludwigs, S. Morphology of P3HT in Thin Films in Relation to Optical and Electrical Properties. In *P3HT Revisited – From Molecular Scale to Solar Cell Devices*; Ludwigs, S., Ed.; Springer Berlin Heidelberg: Berlin, Heidelberg, 2014; Vol. 265, pp 39–82. https://doi.org/10.1007/12_2014_288.
(20) Zhang, W.; Gomez, E. D.; Milner, S. T. Predicting Chain Dimensions of Semiflexible Polymers from Dihedral Potentials. *Macromolecules* **2014**, *47* (18), 6453–6461. https://doi.org/10.1021/ma500923r.
(21) Snyder, C. R.; Kline, R. J.; DeLongchamp, D. M.; Nieuwendaal, R. C.; Richter, L. J.; Heeney, M.; McCulloch, I. Classification of Semiconducting Polymeric Mesophases to Optimize Device Postprocessing. *J. Polym. Sci. Part B Polym. Phys.* **2015**, *53* (23), 1641–1653. https://doi.org/10.1002/polb.23801.
(22) Mollinger, S. A.; Krajina, B. A.; Noriega, R.; Salleo, A.; Spakowitz, A. J. Percolation, Tie-Molecules, and the Microstructural Determinants of Charge Transport in Semicrystalline Conjugated Polymers. *ACS Macro Lett.* **2015**, *4* (7), 708–712. https://doi.org/10.1021/acsmacrolett.5b00314.
(23) Collins, B. A.; Cochran, J. E.; Yan, H.; Gann, E.; Hub, C.; Fink, R.; Wang, C.; Schuettfort, T.; McNeill, C. R.; Chabinyc, M. L.; Ade, H. Polarized X-Ray Scattering Reveals Non-Crystalline Orientational Ordering in Organic Films. *Nat. Mater.* **2012**, *11* (6), 536–543. https://doi.org/10.1038/NMAT3310.
(24) Patel, S. N.; Glaudell, A. M.; Peterson, K. A.; Thomas, E. M.; O'Hara, K. A.; Lim, E.; Chabinyc, M. L. Morphology Controls the Thermoelectric Power Factor of a Doped Semiconducting Polymer. *Sci. Adv.* **2017**, *3* (6), e1700434:1-13. https://doi.org/10.1126/sciadv.1700434.
(25) Gu, K.; Snyder, C. R.; Onorato, J.; Luscombe, C. K.; Bosse, A. W.; Loo, Y.-L. Assessing the Huang–Brown Description of Tie Chains for Charge Transport in Conjugated

Polymers. *ACS Macro Lett.* **2018**, *7* (11), 1333–1338. https://doi.org/10.1021/acsmacrolett.8b00626.
(26) Mei, J.; Bao, Z. Side Chain Engineering in Solution-Processable Conjugated Polymers. *Chem. Mater.* **2014**, *26* (1), 604–615. https://doi.org/10.1021/cm4020805.
(27) Zhou, H.; Yang, L.; You, W. Rational Design of High Performance Conjugated Polymers for Organic Solar Cells. *Macromolecules* **2012**, *45* (2), 607–632. https://doi.org/10.1021/ma201648t.
(28) Han, A.-R.; Lee, J.; Lee, H. R.; Lee, J.; Kang, S.-H.; Ahn, H.; Shin, T. J.; Oh, J. H.; Yang, C. Siloxane Side Chains: A Universal Tool for Practical Applications of Organic Field-Effect Transistors. *Macromolecules* **2016**, *49* (10), 3739–3748. https://doi.org/10.1021/acs.macromol.6b00218.
(29) Kroon, R.; Kiefer, D.; Stegerer, D.; Yu, L.; Sommer, M.; Müller, C. Polar Side Chains Enhance Processability, Electrical Conductivity, and Thermal Stability of a Molecularly p-Doped Polythiophene. *Adv. Mater.* **2017**, *29* (24), 1700930:1-7. https://doi.org/10.1002/adma.201700930.
(30) Zhou, E.; Cong, J.; Hashimoto, K.; Tajima, K. Introduction of a Conjugated Side Chain as an Effective Approach to Improving Donor–Acceptor Photovoltaic Polymers. *Energy Environ. Sci.* **2012**, *5* (12), 9756. https://doi.org/10.1039/c2ee23383e.
(31) Salleo, A.; Kline, R. J.; DeLongchamp, D. M.; Chabinyc, M. L. Microstructural Characterization and Charge Transport in Thin Films of Conjugated Polymers. *Adv. Mater.* **2010**, *22* (34), 3812–3838. https://doi.org/10.1002/adma.200903712.
(32) Kline, R. J.; DeLongchamp, D. M.; Fischer, D. A.; Lin, E. K.; Richter, L. J.; Chabinyc, M. L.; Toney, M. F.; Heeney, M.; McCulloch, I. Critical Role of Side-Chain Attachment Density on the Order and Device Performance of Polythiophenes. *Macromolecules* **2007**, *40* (22), 7960–7965. https://doi.org/10.1021/ma0709001.
(33) Bridges, C. R.; Ford, M. J.; Thomas, E. M.; Gomez, C.; Bazan, G. C.; Segalman, R. A. Effects of Side Chain Branch Point on Self Assembly, Structure, and Electronic Properties of High Mobility Semiconducting Polymers. *Macromolecules* **2018**, *51* (21), 8597–8604. https://doi.org/10.1021/acs.macromol.8b01906.
(34) Zhang, X.; Richter, L. J.; DeLongchamp, D. M.; Kline, R. J.; Hammond, M. R.; McCulloch, I.; Heeney, M.; Ashraf, R. S.; Smith, J. N.; Anthopoulos, T. D.; Schroeder, B.; Geerts, Y. H.; Fischer, D. A.; Toney, M. F. Molecular Packing of High-Mobility Diketo Pyrrolo-Pyrrole Polymer Semiconductors with Branched Alkyl Side Chains. *J. Am. Chem. Soc.* **2011**, *133* (38), 15073–15084. https://doi.org/10.1021/ja204515s.
(35) Noriega, R.; Rivnay, J.; Vandewal, K.; Koch, F. P. V.; Stingelin, N.; Smith, P.; Toney, M. F.; Salleo, A. A General Relationship between Disorder, Aggregation and Charge Transport in Conjugated Polymers. *Nat. Mater.* **2013**, *12* (11), 1038–1044. https://doi.org/10.1038/nmat3722.
(36) O'Connor, B. T.; Reid, O. G.; Zhang, X.; Kline, R. J.; Richter, L. J.; Gundlach, D. J.; DeLongchamp, D. M.; Toney, M. F.; Kopidakis, N.; Rumbles, G. Morphological Origin of Charge Transport Anisotropy in Aligned Polythiophene Thin Films. *Adv. Funct. Mater.* **2014**, *24* (22), 3422–3431. https://doi.org/10.1002/adfm.201303351.
(37) Hamidi-Sakr, A.; Biniek, L.; Fall, S.; Brinkmann, M. Precise Control of Lamellar Thickness in Highly Oriented Regioregular Poly(3-Hexylthiophene) Thin Films Prepared by High-Temperature Rubbing: Correlations with Optical Properties and Charge

Transport. *Adv. Funct. Mater.* **2016**, *26* (3), 408–420. https://doi.org/10.1002/adfm.201504096.
(38) Jimison, L. H.; Toney, M. F.; McCulloch, I.; Heeney, M.; Salleo, A. Charge-Transport Anisotropy Due to Grain Boundaries in Directionally Crystallized Thin Films of Regioregular Poly(3-Hexylthiophene). *Adv. Mater.* **2009**, *21* (16), 1568–1572. https://doi.org/10.1002/adma.200802722.
(39) Chang, J.-F.; Clark, J.; Zhao, N.; Sirringhaus, H.; Breiby, D. W.; Andreasen, J. W.; Nielsen, M. M.; Giles, M.; Heeney, M.; McCulloch, I. Molecular-Weight Dependence of Interchain Polaron Delocalization and Exciton Bandwidth in High-Mobility Conjugated Polymers. *Phys. Rev. B* **2006**, *74* (11), 115318:1-12. https://doi.org/10.1103/PhysRevB.74.115318.
(40) Street, R. A.; Northrup, J. E.; Salleo, A. Transport in Polycrystalline Polymer Thin-Film Transistors. *Phys. Rev. B* **2005**, *71* (16). https://doi.org/10.1103/PhysRevB.71.165202.
(41) Lotz, B.; Miyoshi, T.; Cheng, S. Z. D. *50th Anniversary Perspective* : Polymer Crystals and Crystallization: Personal Journeys in a Challenging Research Field. *Macromolecules* **2017**, *50* (16), 5995–6025. https://doi.org/10.1021/acs.macromol.7b00907.
(42) Martin, D. C.; Chen, J.; Yang, J.; Drummy, L. F.; Kübel, C. High Resolution Electron Microscopy of Ordered Polymers and Organic Molecular Crystals: Recent Developments and Future Possibilities. *J. Polym. Sci. Part B Polym. Phys.* **2005**, *43* (14), 1749–1778. https://doi.org/10.1002/polb.20419.
(43) Brinkmann, M.; Rannou, P. Molecular Weight Dependence of Chain Packing and Semicrystalline Structure in Oriented Films of Regioregular Poly(3-Hexylthiophene) Revealed by High-Resolution Transmission Electron Microscopy. *Macromolecules* **2009**, *42* (4), 1125–1130. https://doi.org/10.1021/ma8023415.
(44) Hartmann, L.; Tremel, K.; Uttiya, S.; Crossland, E.; Ludwigs, S.; Kayunkid, N.; Vergnat, C.; Brinkmann, M. 2D Versus 3D Crystalline Order in Thin Films of Regioregular Poly(3-Hexylthiophene) Oriented by Mechanical Rubbing and Epitaxy. *Adv. Funct. Mater.* **2011**, *21* (21), 4047–4057. https://doi.org/10.1002/adfm.201101139.
(45) Salammal, S. T.; Mikayelyan, E.; Grigorian, S.; Pietsch, U.; Koenen, N.; Scherf, U.; Kayunkid, N.; Brinkmann, M. Impact of Thermal Annealing on the Semicrystalline Nanomorphology of Spin-Coated Thin Films of Regioregular Poly(3-Alkylthiophene)s as Observed by High-Resolution Transmission Electron Microscopy and Grazing Incidence X-Ray Diffraction. *Macromolecules* **2012**, *45* (13), 5575–5585. https://doi.org/10.1021/ma300906v.
(46) Schulz, G. L.; Fischer, F. S. U.; Trefz, D.; Melnyk, A.; Hamidi-Sakr, A.; Brinkmann, M.; Andrienko, D.; Ludwigs, S. The PCPDTBT Family: Correlations between Chemical Structure, Polymorphism, and Device Performance. *Macromolecules* **2017**, *50* (4), 1402–1414. https://doi.org/10.1021/acs.macromol.6b01698.
(47) Fischer, F. S. U.; Kayunkid, N.; Trefz, D.; Ludwigs, S.; Brinkmann, M. Structural Models of Poly(Cyclopentadithiophene- *Alt* -Benzothiadiazole) with Branched Side Chains: Impact of a Single Fluorine Atom on the Crystal Structure and Polymorphism of a Conjugated Polymer. *Macromolecules* **2015**, *48* (12), 3974–3982. https://doi.org/10.1021/acs.macromol.5b00839.
(48) Xue, X.; Chandler, G.; Zhang, X.; Kline, R. J.; Fei, Z.; Heeney, M.; Diemer, P. J.; Jurchescu, O. D.; O'Connor, B. T. Oriented Liquid Crystalline Polymer Semiconductor

Films with Large Ordered Domains. *ACS Appl. Mater. Interfaces* **2015**, *7* (48), 26726–26734. https://doi.org/10.1021/acsami.5b08710.
(49) Zhang, X.; Hudson, S. D.; DeLongchamp, D. M.; Gundlach, D. J.; Heeney, M.; McCulloch, I. In-Plane Liquid Crystalline Texture of High-Performance Thienothiophene Copolymer Thin Films. *Adv. Funct. Mater.* **2010**, *20* (23), 4098–4106. https://doi.org/10.1002/adfm.201001232.
(50) Panova, O.; Chen, X. C.; Bustillo, K. C.; Ophus, C.; Bhatt, M. P.; Balsara, N.; Minor, A. M. Orientation Mapping of Semicrystalline Polymers Using Scanning Electron Nanobeam Diffraction. *Micron* **2016**, *88*, 30–36. https://doi.org/10.1016/j.micron.2016.05.008.
(51) Bustillo, K. C.; Panova, O.; Chen, X. C.; Takacs, C. J.; Ciston, J.; Ophus, C.; Balsara, N. P.; Minor, A. M. Nanobeam Scanning Diffraction for Orientation Mapping of Polymers. *Microsc. Microanal.* **2017**, *23* (S1), 1782–1783. https://doi.org/10.1017/S1431927617009576.
(52) Jiang, X.; Greer, D. R.; Kundu, J.; Ophus, C.; Minor, A. M.; Prendergast, D.; Zuckermann, R. N.; Balsara, N. P.; Downing, K. H. Imaging Unstained Synthetic Polymer Crystals and Defects on Atomic Length Scales Using Cryogenic Electron Microscopy. *Macromolecules* **2018**, *51* (19), 7794–7799. https://doi.org/10.1021/acs.macromol.8b01508.
(53) Takacs, C. J.; Brady, M. A.; Treat, N. D.; Kramer, E. J.; Chabinyc, M. L. Quadrites and Crossed-Chain Crystal Structures in Polymer Semiconductors. *Nano Lett.* **2014**, *14* (6), 3096–3101. https://doi.org/10.1021/nl500150t.
(54) Lovinger, A. J. Microstructure and Unit-Cell Orientation in α-Polypropylene. *J. Polym. Sci. Polym. Phys. Ed.* **1983**, *21* (1), 97–110. https://doi.org/10.1002/pol.1983.180210107.
(55) Lotz, B.; Graff, S.; Wittmann, J. C. Crystal Morphology of the γ (Triclinic) Phase of Isotactic Polypropylene and Its Relation to the α Phase. *J. Polym. Sci. Part B Polym. Phys.* **1986**, *24* (9), 2017–2032. https://doi.org/10.1002/polb.1986.090240909.
(56) Martin, D. C.; Thomas, E. L. Grain Boundaries in Extended-Chain Polymers: Theory and Experiment. *Philos. Mag. A* **1991**, *64* (4), 903–922. https://doi.org/10.1080/01418619108213955.
(57) Ojeda, J. R.; Martin, D. C. High-Resolution Microscopy of PMDA-ODA Polyimide Single Crystals. *Macromolecules* **1993**, *26* (24), 6557–6565. https://doi.org/10.1021/ma00076a038.
(58) Tremel, K.; Fischer, F. S. U.; Kayunkid, N.; Pietro, R. D.; Tkachov, R.; Kiriy, A.; Neher, D.; Ludwigs, S.; Brinkmann, M. Charge Transport Anisotropy in Highly Oriented Thin Films of the Acceptor Polymer P(NDI2OD-T2). *Adv. Energy Mater.* **2014**, *4* (10), 1301659. https://doi.org/10.1002/aenm.201301659.
(59) Trefz, D.; Gross, Y. M.; Dingler, C.; Tkachov, R.; Hamidi-Sakr, A.; Kiriy, A.; McNeill, C. R.; Brinkmann, M.; Ludwigs, S. Tuning Orientational Order of Highly Aggregating P(NDI2OD-T_2) by Solvent Vapor Annealing and Blade Coating. *Macromolecules* **2019**, *52* (1), 43–54. https://doi.org/10.1021/acs.macromol.8b02176.
(60) Lu, X.; Hlaing, H.; Germack, D. S.; Peet, J.; Jo, W. H.; Andrienko, D.; Kremer, K.; Ocko, B. M. Bilayer Order in a Polycarbazole-Conjugated Polymer. *Nat. Commun.* **2012**, *3* (1). https://doi.org/10.1038/ncomms1790.
(61) Prosa, T. J.; Winokur, M. J.; McCullough, R. D. Evidence of a Novel Side Chain Structure in Regioregular Poly(3-Alkylthiophenes). *Macromolecules* **1996**, *29* (10), 3654–3656. https://doi.org/10.1021/ma951510u.

(62) Rivnay, J.; Mannsfeld, S. C. B.; Miller, C. E.; Salleo, A.; Toney, M. F. Quantitative Determination of Organic Semiconductor Microstructure from the Molecular to Device Scale. *Chem. Rev.* **2012**, *112* (10), 5488–5519. https://doi.org/10.1021/cr3001109.
(63) Takacs, C. J.; Treat, N. D.; Kraemer, S.; Chen, Z.; Facchetti, A.; Chabinyc, M. L.; Heeger, A. J. Remarkable Order of a High-Performance Polymer. *Nano Lett.* **2013**, *13* (6), 2522–2527. https://doi.org/10.1021/nl4005805.
(64) Tournebize, A.; Gardette, J.-L.; Taviot-Guého, C.; Bégué, D.; Arnaud, M. A.; Dagron-Lartigau, C.; Medlej, H.; Hiorns, R. C.; Beaupré, S.; Leclerc, M.; Rivaton, A. Is There a Photostable Conjugated Polymer for Efficient Solar Cells? *Polym. Degrad. Stab.* **2015**, *112*, 175–184. https://doi.org/10.1016/j.polymdegradstab.2014.12.018.
(65) Gann, E.; Caironi, M.; Noh, Y.-Y.; Kim, Y.-H.; McNeill, C. R. Diffractive X-Ray Waveguiding Reveals Orthogonal Crystalline Stratification in Conjugated Polymer Thin Films. *Macromolecules* **2018**, *51* (8), 2979–2987. https://doi.org/10.1021/acs.macromol.8b00168.
(66) Chen, H.-Y.; Hou, J.; Hayden, A. E.; Yang, H.; Houk, K. N.; Yang, Y. Silicon Atom Substitution Enhances Interchain Packing in a Thiophene-Based Polymer System. *Adv. Mater.* **2010**, *22* (3), 371–375. https://doi.org/10.1002/adma.200902469.
(67) Panzer, F.; Bässler, H.; Köhler, A. Temperature Induced Order–Disorder Transition in Solutions of Conjugated Polymers Probed by Optical Spectroscopy. *J. Phys. Chem. Lett.* **2017**, *8* (1), 114–125. https://doi.org/10.1021/acs.jpclett.6b01641.
(68) Rivnay, J.; Steyrleuthner, R.; Jimison, L. H.; Casadei, A.; Chen, Z.; Toney, M. F.; Facchetti, A.; Neher, D.; Salleo, A. Drastic Control of Texture in a High Performance N-Type Polymeric Semiconductor and Implications for Charge Transport. *Macromolecules* **2011**, *44* (13), 5246–5255. https://doi.org/10.1021/ma200864s.
(69) Ballauff, M. Stiff-Chain Polymers: Structure, Phase Behavior, and Properties. *Angew. Chem. Int. Ed. Engl.* **1989**, *28* (3), 253–267. https://doi.org/10.1002/anie.198902533.